CrystEngComm

Accepted Manuscript

ROYAL SOCIETY OF CHEMISTRY

www.rsc.org/crystengcomm

Journal Name

RSCPublishing

ARTICLE

Invariant and variable intermolecular interactions in functionalized malonic acid half-esters: X-ray, Hirshfeld surfaces and PIXEL energy analyses†

Perumal Venkatesan,[a] Subbiah Thamotharan,[b] Rajendran Ganesh Kumar[a] and Andivelu Ilangovan[a]*

Cite this: DOI: 10.1039/xoxxoooooox

Received ooth January 2012,
Accepted ooth January 2012

DOI: 10.1039/xoxxoooooox

www.rsc.org/

A series of functionalized malonic acid half-ester derivatives (parent compound **MHE-1**), with variations in functional groups at different positions on the aromatic ring have been synthesized and crystal structures are determined at room temperature (296 K). The methyl (4-CH_3, **MHE-2**) and chloro (4-Cl, **MHE-3**) derivatives are isomorphous with each other. The overall crystal packing of **MHE-1–3** is similar. However, there are few differences observed between stacking of layers in these structures. Compounds with nitro (3-NO_2, **MHE-4**) and ethyl ester (2-$COOC_2H_5$, **MHE-5**) substituent crystallize in different space groups and thus crystal packing is different when compared to **MHE-1-3**. In all the structures, intramolecular N–H...O and O–H…O hydrogen bonds generate two fused *S*(6) rings motif. A detailed study is carried out to visualize intermolecular interactions observed in all five crystal structures (**MHE-1–5**) using Hirshfeld surface (HS) analysis with two dimensional fingerprint plots. The relative contribution of intermolecular H…H contacts in **MHE-3** is substantially lower than that of **MHE-1–2**, though similar crystal packing arrangements of **MHE-1–3** and **MHE-2** and **MHE-3** are isomorphous. From HS analysis it is clear that the observed of H…H contacts contribution (**MHE-3**) is a consequence of the presence of chlorine substituent and growing contribution of Cl…H contacts. The relative contributions of other intermolecular contacts involving various atoms are comparable in **MHE-1–3** structures. The intermolecular interaction energies are quantified using PIXEL for various molecular pairs extracted from respective crystal structures. Interestingly, there are some invariant and variable intermolecular contacts observed between different groups in all five structures.

Introduction

Study of non-covalent interactions and their control is considered to be an important subject in the field of crystal engineering,[1] to design a material of desirable properties.[1] The non-covalent interactions are broadly classified based on their energies into strong (15-40 kcal/mol), moderate (4-15 kcal/mol) and weak (≤ 4 kcal/mol). Especially, the weaker interactions such as C–H...O, C–H...π and π...π form the basis for the design of the supramolecular association in organic crystals, molecular recognition processes, polymorphism and complicated crystal packing.[2-3] It has been reported that the weaker interactions are dominant in the absence of stronger hydrogen bonds[4] and sometimes they provide additional stability to the crystal structure. Therefore, it is of vital importance to study the interplay of non-covalent interactions associated in the crystal structure as well as to study the structural features of the molecule.

In the present work, we have synthesized a series of functionalized malonic acid half-ester derivatives and their crystal structures have been determined using single crystal X–ray analysis. Half-esters, which contain both acid and ester functional groups, can be classified as geminal, vicinal, vinylic, aromatic and simple half-ester depend on acid and ester

[a] School of Chemistry, Bharathidasan University, Tiruchirappalli 620024, Tamilnadu, India. Fax +91- 431 2407045 /2412750; Tel: +91-98654 36093; Email: ilangovanbdu@yahoo.com
[b] Department of Bioinformatics, School of Chemical and Biotechnology, SASTRA University, Thanjavur 613 401, Tamilnadu, India.

†Electronic Supplementary Information (ESI) available: Synthetic procedures for compounds **MHE-1–5.** Crystal packing arrangements in **MHE-1–5**(Fig. S1) and DFT-optimized structures (Fig. S2), structural superimposition diagrams (Fig. S3), part of crystal structure displaying various intermolecular interactions (Fig. S3–11), the shape index and curvedness diagrams for structures **MHE-1–5** (Fig. S12–13) and various fragments in **MHE-1–3**, which are used for the CSD search highlighted in different colours (Fig. S14), The CIF files can also be obtained from the Cambridge Crystallographic Data Centre (CCDC) and CCDC reference numbers 832627, 957106, 957107, 957109 and 957110.

moieties substitution positions. The structures which are discussed in the present study fall under the class of germinal half-ester. Malonic acid half-esters are widely known germinal half-esters which find extensive applications as intermediates in organic synthesis.[5] Similarly, half-esters are part of the core in biologically active natural products and valuable chemicals.[6-9] It has been reported that some of the half-esters are part of the structure in commercial drugs such as trandolapril[10] and artesunate.[11] The former drug acts as an ACE (Angiotension Converting Enzyme) inhibitor to treat high blood pressure, while the latter being used to treat malaria. Because of this biological relevance of half-ester derivatives, we investigate the crystal structures of five malonic acid half-ester (**MHE-1–5**) derivatives and various intermolecular interactions present in them.

A detailed study has been carried out to visualize intermolecular interactions present in respective crystal structures using HS analysis[12] along with decomposed two dimensional fingerprint plots.[13] Hirshfeld surfaces are useful to identify the differences in the intermolecular contacts between different crystal structures. The lattice energies of the crystal structures are calculated using PIXEL[14] and various intermolecular interactions present in different molecular pair are quantified. Furthermore, the crystal structures are optimized in gas-phase using DFT/BL3YP/6-311G++** level of theory[15] and the structural features of molecules derived from experimental and theoretical calculations are also compared.

Experimental

General experimental procedure for the synthesis of malonic acid half-ester derivatives MHE-1–5

Malonic acid half-ester derivatives (**MHE-1**–**5**) were prepared by $BF_3.OEt_2$ mediated hydrolysis of germinal diester as reported earlier (Scheme 1).[16] Briefly, to a solution of 2-[(arylamino) methylene] malonic acid diethyl ester (1.0 equiv.) in $CHCl_3$ (3x w/v) and $BF_3.OEt_2$ (1.0 equiv.) was added and stirred at 296 K. Completion of the reaction was determined by TLC. The reaction mixture was quenched with water (1x w/v) and then extracted with $CHCl_3$ (3x10 mL). The combined organic layer was dried (anhyd. Na_2SO_4) and evaporated in rotary evaporator under vacuum. The crude product obtained was passed through a short silica gel column using a suitable eluent to get corresponding product.

[Insert Scheme 1]

Single crystal X-ray diffraction

All datasets were collected at 296 K on a Bruker SMART APEXII CCD diffractometer[17] using *Mo Kα* radiation (λ = 0.71073 Å). Data collected from weakly diffracting crystals (**MHE-2** and **MHE-4**) that showed no intensity data beyond 24° and experimental limitations prevented collecting for longer measurement time. All the structures except **MHE-3** were solved by direct methods using the program SHELXS-2013.[18] Since the 4-CH_3 derivative (**MHE-2**) is isomorphous with the 4-Cl derivative (**MHE-3**), the structure of **MHE-3** was refined with the coordinates of non-hydrogen atoms after removing *para*-methyl (4-CH_3) carbon of **MHE-2**. The position of the Cl atom substituted at the *para* position was determined from a difference Fourier map and refined anisotropically. All the non-hydrogen atoms were refined by full-matrix least-squares on F^2 using SHELXL-2014/6.[18] In all the structures, the methyl H atoms were constrained to an ideal geometry (C–H = 0.98 Å) with U_{iso}(H) = 1.5U_{eq}(C), but were allowed to rotate freely about the C–C bond. The remaining H atoms were placed in geometrically calculated positions (C–H = 0.95 Å) and constrained to ride on their parent atoms with U_{iso}(H) = 1.2U_{eq}(C). The position of amine and hydroxy H atom was located from difference electron density maps and refined freely along with its isotropic displacement parameters. The thermal ellipsoidal plot and crystal packing diagrams were generated using the programs ORTEP-3,[19] PLATON[20] and MERCURY.[21] The crystal data, details of the data collection and refinement statistics are summarized in Table 1. The selected torsion angles are given in the electronic supplementary information (Table S1, ESI†). The hydrogen-bonding parameters are given in Table 2. The crystal packing of these molecules was analyzed using the software XPac 2.0.[22] The details of XPac analysis and the crystal packing diagrams for **MHE-1–5** are given (Section 4 and Fig. S1, ESI†).

Quantum chemical calculation

The starting structure for the gas phase geometry optimization was taken from respective crystal structure. The molecular geometry and vibrational frequencies of the structures in the ground state were calculated using the Density Functional Theory (DFT) method with BL3YP/6-311G++** basis set.[15] The resulting geometrical parameters were compared with those of structures obtained from X–ray crystallography and the optimized structures are given (Fig. S2, ESI†). All the computations were performed using Jaguar[23] module implemented in Schrödinger suite.[24] All the optimized structures were confirmed to be energy minima on the potential energy surface through vibrational frequency calculations.

Hirshfeld surface analysis and PIXEL energy calculation

A systematic analysis was carried out to investigate various intermolecular interactions including O…H, H…H, C…H, C…C, H…Cl and other types of non-covalent contacts presented in crystal structures of **MHE-1–5** using CrystalExplorer 3.1.[25] With the aid of decomposed two dimensional fingerprint plots,[13] one can quantify and visualize the intermolecular interactions involved in the crystal packing. Briefly, HS was constructed for a molecule in the crystal environment mapped with different properties such as d_e (distance from the HS to the nearest atom outside the surface), d_i (distance from the HS to the nearest atom inside the surface), d_{norm} (normalized contact distance), shape index and curvedness to analyse intermolecular interactions. The bond lengths (C–H

= 1.083 Å, N–H = 1.009 Å and O–H = 0.983 Å) were adjusted to typical neutron diffraction values before the HS calculation. In HS diagrams, the contacts with distances equal to the sum of the van der Waals radius are indicated as white and the contacts with distances shorter than and longer than van der Waals radii are represented as red and blue, respectively. The normalized distance d_{norm} can be calculated using the following formula

$$d_{norm} = \frac{d_i - r_i^{vdW}}{r_i^{vdW}} + \frac{d_e - r_e^{vdW}}{r_e^{vdW}}$$

For all the structures, the lattice energy which partitioned into Coulombic, polarization, dispersion and repulsion contributions was calculated using PIXEL module in the CLP (Coulomb-London-Pauli) program.[14] The CLP model is a theoretical approach to evaluate intermolecular potentials. It assumes any intermolecular potential can be divided into a Coulomb-polarization term, a dispersion term (London) and a repulsion term (Pauli). Before the calculation, distances involving hydrogen atoms were moved to their neutron values and an electron density of the molecules were calculated at MP2/6-31G** with Gaussian 09 package.[26] The molecular pairs held together by various non-covalent interactions were carefully selected from respective crystal structures based on interaction energies. The interaction energies of various molecular pairs in all five crystal structures (**MHE-1–5**) were listed in Table 3.

Results and discussion

In the present study, we have synthesized a series of malonic acid half-ester derivatives, **MHE-1–5** and their crystal structures have been examined to understand how different functional groups substituted at different positions on the aromatic ring alter the crystal packing. The ORTEP diagrams of all five compounds are displayed in Fig.1.

Table 1. Crystal data and refinement details

Compound	**MHE-1**	**MHE-2**	**MHE-3**	**MHE-4**	**MHE-5**
Empirical formula	C_{12} H_{13} N O_4	C_{13} H_{15} N O_4	C_{12} H_{12}Cl N O_4	C_{12} H_{12} N_2 O_6	C_{15} H_{17} N O_6
Formula weight	235.23	249.26	269.68	280.24	307.30
T (K)	296(2)	296(2)	296(2)	296(2)	296(2)
Wavelength (Å)	0.71073	0.71073	0.71073	0.71073	0.71073
Crystal system	Triclinic	Triclinic	Triclinic	Monoclinic	Monoclinic
Space group	PĪ	PĪ	PĪ	P2(1)/c	P2(1)/n
a (Å)	7.0418(13)	6.8768(2)	7.0837(2)	11.4230(7)	7.9000(2)
b (Å)	7.5275(14)	7.5092(3)	7.4404(2)	8.6148(5)	23.1582(7)
c (Å)	11.444(2)	12.8653(4)	12.4791(4)	13.9893(9)	8.7135(2)
α (°)	84.212(9)	93.415(2)	92.127(2)	90.00	90.00
β (°)	75.935(9)	104.473(2)	105.123(2)	112.165(4)	107.9040(10)
γ (°)	82.835(9)	95.382(2)	97.607(2	90.00	90.00
V (Å^3)	582.28(18)	638.06(4)	627.58(3)	1274.91(14)	1516.93(7)
Z	2	2	2	4	4
Calculated density (Mg/m^3)	1.342	1.297	1.427	1.460	1.346
Absorption (mm^{-1})	0.102	0.097	0.310	0.119	0.105
F(0 0 0)	248	264	280	584	648
Crystal size (mm)	0.22 × 0.16 × 0.14	0.40 × 0.30 × 0.20	0.12 × 0.12 × 0.08	0.23 × 0.20 × 0.18	0.28 × 0.13 × 0.11
θ (°)	1.84–33.58	1.64–24.32	1.70–32.04	1.93–23.72	1.76–29.63
Limiting indices	−10 ⩽ h ⩽ 10, −11 ⩽ k ⩽ 11, −16 ⩽ l ⩽ 16	−7 ⩽ h ⩽ 7, −8 ⩽ k ⩽ 8, −14 ⩽ l ⩽ 14	−10 ⩽ h ⩽ 10, −10 ⩽ k ⩽ 11, −18 ⩽ l ⩽ 18	−12 ⩽ h ⩽ 12, −9 ⩽ k ⩽ 9, −15 ⩽ l ⩽ 13	−9 ⩽ h ⩽ 10, −32 ⩽ k ⩽ 32, −12 ⩽ l ⩽ 9
Reflections collected/unique (Rint)	14267/2736 (0.0220)	9589/1479 (0.0291)	14717/2845 (0.0291)	9184/1490 (0.0214)	18031/ 2519 (0.0283)
(θ °) Completeness (%)	(25.0) 100.0	(24.32) 100.0	(25.0) 100.0	(23.72) 99.7	(29.63) 99.7
Refinement method F^2	full-matrix least-squares on F^2	full-matrix least-squares on F^2	full-matrix least-squares on F^2	full-matrix least-squares on F^2	full-matrix least- squares on F^2
Data/restraints /parameters	2736/0/163	1479/0/173	2845/0/172	1490/0/191	2519/0/ 210
Goodness-of-fit(GOF) onF^2	1.035	1.071	1.048	1.033	1.038
Final R indices [I > 2σ(I)]	R1 = 0.0473, wR2 = 0.1314	R1 = 0.0392, wR2 = 0.0958	R1 = 0.0493, wR2 = 0.1421	R1 = 0.0391, wR2 = 0.0937	R1 = 0.0522, wR2 = 0.1419
R indices (all data)	R1 = 0.0692, wR2 = 0.1492	R1 = 0.0616, wR2 = 0.1077	R1 = 0.0722, wR2 = 0.1634	R1 = 0.0538, wR2 = 0.1020	R1 = 0.0902, wR2 = 0.1656
Largest difference in peak and hole (e A^{-3})	0.245 and -0.240	0.149 and -0.153	0.603 and -0.416	0.304 and -0.248	0.421 and -0.253

[Insert Figure 1]

Fig. 1 A view of the asymmetric unit showing the atomic numbering scheme. The atomic displacement plots have been drawn at 50% probability level for compounds (a) **MHE-1**, (b) **MHE-2**, (c) **MHE-3**, (d) **MHE-4** and (e) **MHE-5**.

The compounds **MHE-1**–**3** crystallize in the triclinic space group $P\bar{1}$ with $Z = 2$. The unit cell dimensions are comparable in **MHE-1**–**3**, where α, β and γ angles are slightly deviated in the parent compound (**MHE-1**, see Table 1). It is of interest to note that the structure of **MHE-2** is isomorphous with **MHE-3**, while **MHE-1** is not. Compounds **MHE-4** with 3-NO_2 group and **MHE-5** with 2-$COOC_2H_5$ functional are crystallized in monoclinic space groups $P2_1/c$ and $P2_1/n$ respectively with $Z = 4$. All the five compounds **MHE-1**–**5** have a common skeletal framework consisting of acid and ester groups at geminal position and an N-vinyl aniline moiety. The structural superimposition is carried out to identify the conformational changes on the molecular structure upon different substitutions. The common atoms (N1/C7/C8/C9/O2/O1/C10/O3/O4/C11/C12) in **MHE-1**–**5** are used for structural superimposition (Fig.2).

[Insert Figure 2]

Fig. 2 Structural superimposition of crystal structures involving common atoms (N1/C7/C8/C9/O2/O1/C10/O3/O4/C11/C12). The colour codes is **MHE-1** (red), **MHE-2** blue), **MHE-3** (magenta), **MHE-4** (green) and **MHE-5** (cyan).

The maximum RMSD (root mean square deviation) between any molecular pair is 0.067 Å (for **MHE-1** and **MHE-5** pair). The structural superimposition diagrams indicate that the phenyl ring in **MHE-4**–**5** adopts different orientations when compared to other three structures **MHE-1**–**3**. The complete details of the structural superimposition comparisons are given (Section 3, ESI†). The dihedral angles between different mean planes for all these molecules are listed (Table S2, ESI†). In all the optimized structures, the orientation of the phenyl ring is the same as observed in crystal structures. The selected torsion angles (C7– N1–C1–C2 and C7–N1–C1–C6) obtained from DFT calculations are compared with the crystal structure values to assess the phenyl ring orientation (Table S1, ESI†). However, the values are deviating by 10–20° from the crystal structure geometry.

In all five structures, amine and hydroxy groups act as donors and carbonyl groups (atoms O2 and O3) of geminal half-ester and acid moieties act as acceptors. In addition, the 3-NO_2 (in **MHE-4**) and 2–$COOC_2H_5$ (in **MHE-5**) substituent groups also act as acceptors for intermolecular interactions. Two invariant intramolecular N–H…O and O–H…O hydrogen bonds are observed in all five structures (Table 2) which produce two fused $S(6)$ motifs.[27] In **MHE-5**, an additional intramolecular N–H…O hydrogen bond is observed between amine and carbonyl group of 2–$COOC_2H_5$ substituent group. This additional intramolecular hydrogen bond combines with two invariant intramolecular hydrogen bonds which generate a chain of three fused $S(6)$ ring systems (Fig. 1 and Fig. S4, ESI†). Interestingly, in **MHE-1**–**3**, an invariant intermolecular N–H…O hydrogen bond is observed between C=O of the carboxylic acid and N–H group which produces a molecular dimer with $R_2^2(12)$ motif (Fig. 3(A)). A CSD search[28-29] (search filters: R-factor: ≤ 0.5%, not disordered and only organic) for the existence of $R_2^2(12)$ motif with $(H1–N1–C7=C8–C9=O2)_2$ fragments as a template. We found that there are 156 hits with this motif. The fragments used for CSD search are highlighted (Fig. S14, ESI†).

It is of interest to note that the presence of methyl group in **MHE-2** and chloro substitution in **MHE-3** does not alter the invariable intermolecular N–H…O hydrogen bond (Fig. S5–6, ESI†). The interaction energy for this dimer is found to be similar in **MHE-1** and **MHE-2** (−12.5 kcal/mol for **MHE-1** and −12.3 kcal/mol for **MHE-2**, Table 3), whereas it is slightly stronger in **MHE-3** (−15.0 kcal/mol). This is also reflected in the overall lattice energy (−29.3 kcal/mol for **MHE-1**, −29.5 kcal/mol for **MHE-2** and −32.5 kcal/mol, Table 4). These differences mainly arise due to the contribution of Coulombic energy. Within an intermolecular N–H…O dimer, carbonyl…carbonyl (C9=O2…O2=C9) contact is also observed. A CSD search indicates that there are 48 hits with this contact in addition to N–H…O intermolecular hydrogen bond. The carbonyl…carbonyl contact is observed with a range of 2.766 − 3.036 Å with an average of 2.94 Å. In **MHE-1**–**3**, this contact is observed with a range of 2.789 − 2.851 Å. This dimeric molecular pair is further stabilized by an intermolecular C2–H2…O2 interaction with $R_2^2(16)$ motif. This interaction along with an intermolecular N–H…O hydrogen bond is only found in **MHE-1**–**3**. As shown in Fig.3(A), two adjacent N–H…O/C–H…O molecular dimers are interconnected through ester moieties (C11…O3=C10) and the interaction energy (~ −5.5 kcal/mol, Table 3) for this molecular pair is found to be almost the same as that observed in **MHE-1**–**3**. The invariant C2–H2…O2 and C11…O3=C10 contacts are clearly visible on the Hirshfeld surfaces of **MHE-1**–**3** (Fig.4). A CSD search suggests that this type of contact is seen in 63 crystal structures. Overall, the above mentioned interactions generate a molecular ribbon like arrangement (Fig S5–6, ESI†) in crystal structures of **MHE-1**–**3** and these is no significant effect observed due to presence of aromatic substituents. However, the stacking of the layers differs somewhat in these structures (Fig S7–9, ESI†). The N–H…O molecular dimers are related by center of inversion in adjacent layers and are interconnected by C8…C9 contacts (Fig 3(B)). It is worth mentioning that this contact is

shorter than the sum of the van der Waals radii of atoms C8 and C9 in **MHE-2** while this contact is slightly longer (sum of the van der Waals radii + 0.1 Å) in **MHE-1** and **MHE-3**.

Table 2. Various intra- and intermolecular interaction observed in structures of **MHE-1–5** and key contacts visible on the HS are labelled. *-indicates the centroid-to-centroid distance and centroid is formed by atoms C1–C6.

Compound	D–H···A	D–H	H···A	D···A	D–H···A	Symmetry	Label
MHE-1	O1–H1O···O3=C10	0.90(2)	1.67(2)	2.5281(13)	159(2)		
	N1–H1N...O2=C9	0.870(17)	2.089(16)	2.7072(13)	127.4(13)		
	N1–H1N ···O2=C9	0.870(17)	2.326(17)	3.1340(14)	154.5(13)		1
	C2–H2…O2=C9	0.93	2.68	3.3483(16)	129.2	1–x, 1–y, 1–z	2
	C9=O2…O2=C9			2.789			3
	C11…O3=C10			3.1822(16)		–x–1, –y+2, 1–z	4
	C8...C9			3.449		–x, 1–y, 1–z	
	C11–H11A…O1–C9			3.889		–x, –y+2, 1–z	
	π... π stacking			4.280*		–x, 1–y, –z+2	
MHE-2	O1–H1O...O3=C10	0.94(3)	1.65(3)	2.5356(19)	155(2)		
	N1–H1N···O2=C9	0.90(2)	2.05(2)	2.713(2)	129.2(19)		
	N1–H1N···O2=C9	0.90(2)	2.28(2)	3.092(2)	149.9(19)		1
	C2–H2...O2=C9	0.93	2.65	3.301(2)	127.4	1–x, 1–y,1–z	2
	C9=O2…O2=C9			2.814			3
	C8…C9			3.352(2)		–x, 1–y, 1–z	4
	C11…O3=C10			3.149		–x –1, –y, 1–z	5
	C11–H11A…O1–C9			3.803		–x, –y, 1–z	
	π... π stacking			4.514*		1–x, 1–y, –z+2	
MHE-3	O1–H1O...O3=C10	0.86(2)	1.71 (2)	2.5343(16)	158(2)		
	N1–H1N...O2=C9	0.92(2)	2.05(2)	2.7059(17)	127(19)		
	N1–H1N...O2=C9	0.92(2)	2.31(2)	3.1512(16)	151.3(19)		1
	C2–H2...O2=C9	0.93	2.56	3.265(2)	132.8	1–x, 1–y,1–z	2
	C9=O2…O2=C9			2.851			3
	C11…O3=C10			3.154		–x –1, –y, 1–z	4
	C8…C9			3.402		–x,1–y,1–z	
	π... π stacking			4.341*		1–x,1–y, –z+2	
	C11–H11A…O1–C9			3.882		–x, –y, 1–z	
MHE-4	O1–H1O...O3=C10	0.89(3)	1.70(3)	2.554(2)	160(3)		
	N1–H1N...O2=C9	0.86(2)	2.01(2)	2.677(2)	133(2)		
	C6–H6...O2=C9	0.93	2.56	3.362(2)	145	x, 1/2−y, −1/2+z	1
	N1–H1N...O5=N2	0.86(2)	2.54(2)	3.130(2)	126.4(17)	1−x, 1/2+y, 3/2−z	2
	C4–H4...O6=N2	0.93	2.47	3.328(3)	154	1−x, −1 −y, 1−z	3
	C5–H5...O5=N2	0.93	2.50	3.178(3)	130	x, −1/2 −y, 1/2 + z	4
	C10=O3… C9–O1			3.264		-x,1-y,1-z	
	π... π stacking			3.604*		1-x, -y, 1-z	
MHE-5	O1–H1O...O3=C10	0.87(4)	1.72(2)	2.553(2)	158(4)		
	N1–H1N···O2=C9	0.84(2)	2.13(2)	2.7163(19)	127.2(18)		
	N1–H1N···O5	0.84(2)	2.04(2)	2.709(2)	137(2)		
	C7–H7…O3=C10	0.93	2.62	3.265(2)	127.1	–1/2+x, 1/2–y, –1/2+z	1
	C11–H11B…O2=C9	0.97	2.61	3.376(3)	136.1	1/2+x,1/2–y, –1/2+z	2
	C14–H14A…Cg1	0.970	2.93	3.810(3)	152	1–x, –y,1–z	
	π... π stacking			4.568*		–x+2, –y, 1–z	
	C15– H15B …O1	0.960	2.864(2)	3.415(4)	117.59(2)	–x+2, –y, –z+2	
	C5–H5…O5	0.930	2.758(1)	3.643(2)	159.34(11)	x, y, 1+z	

[Insert Figure 3]

Fig. 3 Part of the crystal structures (**MHE-1–3**) showing various intermolecular interactions (A) a molecular ribbon arrangement in **MHE-1**; (B) adjacent layers are interconnected by C8…C9 contacts in **MHE-2**.

Table 3. Interaction energies (E_{Tot}) partitioned into Coulombic (E_{Coul}), polarization (E_{Pol}), dispersion (E_{Disp}) and repulsion (E_{rep}) contributions (in kcal/mol) for various molecular pairs in **MHE-1–5**.

Centroids distance	E_{Coul}	E_{Pol}	E_{Disp}	E_{Rep}	E_{Tot}	Symmetry	Important Interactions
MHE-1							
6.975	–11.5	–4.4	–6.6	10.0	–12.5	1–x, 1–y, 1–z	N1–H1*N*···O2=C9; C2–H2...O2=C9; C9=O2…O2=C9
4.642	–6.2	–1.8	–9.4	5.7	–11.8	–x, 1–y, 1–z	C8...C9
6.997	–3.7	–1.1	–5.7	2.8	–7.7	–x, –y+2, 1–z	C11 – H11*A*…O1=C9
7.243	–1.3	–0.9	–9.6	5.3	–6.5	–x, 1–y, –z+2	π... π stacking
10.382	–4.0	–1.0	–4.3	3.7	–5.6	–x-1, –y+2, 1–z	C11…O3=C10
MHE-2							
7.005	–11.3	–4.6	–6.9	10.5	–12.3	1–x, 1–y,1–z	N1–H1*N*···O2=C9; C2–H2...O2=C9; C9=O2…O2=C9
5.309	–5.9	–1.8	–9.1	6.0	–10.9	–x,1–y,1–z	C8...C9
7.544	–4.0	–1.2	–6.0	3.2	–7.9	–x, –y, 1–z	C11– H11*A*…O1=C9
10.997	–3.9	–0.9	–4.2	3.5	–5.5	–x –1, –y, 1–z	C11…O3=C10
7.967	–0.5	–1.3	–9.0	6.1	–4.7	1–x, 1–y, –z+2	π... π stacking
MHE-3							
7.226	–13.4	–4.9	–7.2	10.4	–15.0	1–x, 1–y,1–z	N1–H1*N*···O2=C9; C2–H2...O2=C9; C9=O2…O2=C9
5.956	–6.2	–1.7	–9.1	5.4	–11.6	–x,1–y,1–z	C8...C9
6.804	–2.7	–1.1	–10.6	6.4	–8.0	1–x,1–y, –z+2	π... π stacking
8.426	–3.9	–1.0	–5.7	2.7	–7.9	–x, –y, 1–z	C11– H11*A*…O1=C9
11.859	–3.9	–1.0	–4.2	3.5	–5.5	–x –1, –y,1–z	C11…O3=C10
MHE-4							
8.330	–4.9	–1.1	–5.8	2.7	–9.1	–x,1–y,1–z	C11…C9; C9…O3; C11–H11*B*…O2=C9
6.059	–2.4	–0.8	–8.9	4.0	–8.1	1–x, –y, 1–z	π... π stacking
7.109	–4.2	–1.5	–4.9	3.1	–7.4	x, 1/2−y, −1/2+z	C6–H6...O2=C9
8.042	–4.5	–1.3	–4.3	3.8	–6.3	1−x, 1/2+y, 3/2−z	N1–H1*N*...O5=N2
12.778	–4.5	–1.0	–2.9	3.6	–4.8	1−x, −1 −y, 1−z	C4–H4...O6=N2
10.143	–1.0	–0.5	–1.7	1.8	–1.3	x, −1/2 −y, 1/2+ z	C5–H5...O5=N2
MHE-5							
5.183	–2.7	–1.6	–16.3	7.9	–12.7	–x+2, –y, 1–z	π... π stacking
9.158	–5.0	–1.6	–3.2	2.2	–7.5	–x+2, –y, –z+2	C15–H15*B*…O1–C9
8.052	–1.9	–0.8	–7.8	3.5	–7.0	1–x, –y, 1–z	C14–H14*A*…Cg1
8.714	–2.9	–1.3	–3.9	2.6	–5.6	x, y, 1+z	C5–H5…O5
8.279	–0.8	–1.2	–6.9	4.0	–4.9	–1/2+x, 1/2–y, –1/2+z	C7–H7…O3=C10
9.471	–1.7	–1.0	–4.0	2.6	–4.0	1/2+x, 1/2–y, –1/2+z	C11–H11*B*…O2=C9

[Insert Figure 4]

Fig. 4 Views of the Hirshfeld surfaces mapped with d_{norm} in two different orientations for **MHE-1**–**5**. The default values are taken for colour codes (red and blue). Refer Table 2 for the numbered arrows.

Journal Name RSCPublishing

ARTICLE

As shown in Table 3, the interaction energy for this molecular pair is nearly the same in all three structures **MHE-1–3**. An yet another key invariant intermolecular interaction C11–H11*A*…O1–C9 links the adjacent layers which is observed between ester moiety (C11 atom) in one layer and hydroxy group (O1 atom) of an acid moiety in an adjacent layer (Fig S10, ESI†). The interaction energy for this molecular pair is nearly the same in these three structures (–7.7 kcal/mol for **MHE-1**, –7.9 kcal/mol for **MHE-2** and –7.9 kcal/mol for **MHE-3**). However, this intermolecular contact is longer than the sum of the van der Waals radii. This intermolecular contact is established within a sum of the van der Waals radii plus 0.2 Å criterion. In addition to these interactions, adjacent layers are also interlinked by an π…π stacking interaction (Fig. S7–9, ESI†). The phenyl rings centroid to centroid distance is 4.280 Å in **MHE-1**, 4.514 Å in **MHE-2** and 4.314 Å in **MHE-3**. The interaction energy for the corresponding molecular pair being –6.5 kcal/mol in **MHE-1**, –4.7 kcal/mol in **MHE-2** and –8.0 kcal/mol in **MHE-3** (see Table 3). It should be noted that the centroids distance of the π…π stacked molecular pair (with this pair, for each whole molecule, a centroid point is calculated and then distance is calculated between these centroids), based on PIXEL calculation, is shorter (6.804 Å) in **MHE-3**, whereas the centroids distance is little longer in **MHE-1**–**2** (7.243 Å in **MHE-1** and 7.967 Å in **MHE-2**).

The differences in interaction energies and the centroids distances of molecular pairs collectively suggest that the layers are tightly packed in **MHE-3** when compared to **MHE-1**–**2**. It is also evident from the overall lattice energies for these three structures (Table 4). It is found that the overall lattice energy is stronger for **MHE-3** when compared to **MHE-1**–**2** structures. It is of worthy to note that even though variations observed in stacking of layers, non-covalent contacts observed between different functional groups are invariant in **MHE-1**–**3.** For example, acid/acid (O2…O2), phenyl ring/acid (C2–H2…O2), ester/ester (C11…O3) and ester/acid (C11–H11A…O1). Using HS, the intermolecular contacts are analysed in detail (Fig. 4) and key contacts are indicated by arrows with number. The full two dimensional fingerprint plots, decomposed fingerprint plots and relative contributions of various intermolecular interactions to the Hirshfeld surface area of all five structures are depicted in Figs. 5–6. It is clearly visible in Fig. 6 that the H…H contacts are dominant in **MHE-2** (49%) and are relatively comparable in **MHE-1** (44.2%). However, H…H intermolecular contacts are drastically reduced in **MHE-3**. This drastic reduction may due to the presence of chlorine atom at the *para* position on the phenyl ring which makes about 16.4% with hydrogen atoms (Cl…H). The relative contributions for intermolecular contacts involving other atoms such as O…O, O…H, O…C and C…C are comparable in these three structures (**MHE-1**–**3**).

[Insert Figure 5]

Fig. 5 The decomposed two dimensional fingerprint plots for **MHE-1–5**. Various close contacts and their relative contributions are indicated. The arrow mark indicates the H…Cl contact observed in **MHE-3**.

[Insert Figure 6]

Fig. 6 Relative contributions to Hirshfeld surface (HS) areas for various intermolecular contacts in **MHE-1**–**5**.

The oxygen atoms of the nitro group act as good acceptors for weak hydrogen bonds in many compounds with nitrobenzene functionality.[3] These weak hydrogen bonds play an pivotal important role in crystal packing of nitrobenzene and nitroaniline compounds.[30] The nitro group also participates in electrostatic interaction between negatively charged oxygen atoms and positively charged nitrogen atoms.[31] As observed in many structures,[30] the nitro group acts as an acceptor for weak intermolecular interactions in **MHE-4**. In this structure, apart from invariant intramolecular N–H…O and O–H…O hydrogen bonds, intermolecular N–H…O and C–H…O interactions are also observed. Interestingly, an intermolecular hydrogen bond forms between amine (N–H) and carbonyl (O2=C9) moiety is altered due to the presence of meta nitro substitution on the phenyl ring. However, the amine group acts as a donor for an intermolecular N–H…O hydrogen bond with atom O5 of nitro

group of neighbouring molecule and it links the molecules as a parallel double layer which runs parallel to the b axis that has a graph set motif of $C(7)$ (Fig. 7) with the interaction energy is being –6.3 kcal/mol. The intermolecular N–H…O hydrogen bond between amine and meta nitro is searched in the CSD. This type of interaction is found only in 11 hits (the maximum H…O distance: 2.716 Å, the minimum H…O distance: 2.181 Å and average H…O distance: 2.448 Å). In **MHE-4**, the H…O5 distance being 2.540 Å.

[Insert Figure 7]

Fig. 7 Part of the crystal structure of **MHE-4**, showing the formation of hydrogen-bonded $C(7)$ chain which runs parallel to the *b* axis.

[Insert Figure 8]

Fig. 8 Part of the crystal structure of **MHE-4**, showing the formation of alternate $R_2^2(10)$ and $R_3^3(14)$ rings generated from intermolecular N–H…O and C–H…O interactions.

Table 4. Lattice energies (kcal/mol) partitioned into Coulombic, polarization, dispersion and repulsion contributions for **MHE-1**–**5**.

Compound	E_{coul}	E_{pol}	E_{Disp}	E_{rep}	E_{Tot}
MHE-1	–13.7	–4.4	–30.9	19.8	–29.3
MHE-2	–13.0	–4.9	–32.1	20.5	–29.5
MHE-3	–14.5	–4.8	–34.2	20.9	–32.5
MHE-4	–14.7	–4.7	–32.5	18.8	–33.1
MHE-5	–12.3	–4.2	–35.3	18.0	–33.8

[Insert Figure 9]

Fig. 9 Part of the crystal structure of **MHE-4**, showing the formation of tetrameric molecular arrangement giving rise to $R_4^4(26)$ rings generated from intermolecular N–H…O and C–H…O interactions. The ring centroid positions of the central molecules are represented as spheres.

In addition to intra and intermolecular hydrogen bonds, three intermolecular C–H…O interactions are also observed. The intermolecular C4–H4…O6 interaction forms a molecular dimer with $R_2^2(10)$ motif (Fig. 8) and an another intermolecular C5–H5…O5 interactions links the molecules into a $C(6)$ chain which runs parallel to the *c* axis. As shown in Fig. 8, the intermolecular N1–H1N…O6, C4–H4…O6 and C5–H5…O5 interactions collectively form $R_3^3(14)$ ring architecture. Overall, these interactions generate an alternate $R_3^3(14)$ and $R_2^2(10)$ rings. The intermolecular C6–H6…O2 interaction links the molecules into a $C(7)$ chain which runs parallel to the *b* axis. Among these three intermolecular C–H…O interactions, C6–H6…O2 interaction is stronger and C5–H5…O5 is weaker (Table 3). The intermolecular N1–H1N…O5 and C6–H6…O2 interactions combine to generate an $R_4^4(26)$ motif (Fig. 9). Within this tetrameric arrangement, two phenyl rings from symmetry related molecules (*x, y, z and –x+1, –y, –z+1*) are making a π…π stacking interaction with a centroid-to-centroid distance of 3.604 Å (Fig. 9). It is of interest to note that the interaction between π…π stacking molecular pair is stronger than molecular pairs stabilized by intermolecular C–H…O interactions (Table 3).

Another interesting key intermolecular contact is observed in **MHE-4**. In this contact, carbonyl group (C10 and O3 atoms) of the ester moiety is stacked with carboxylic acid moiety (O1 and C9 atoms, see Fig. S11, ESI†). This contact is not visible on the Hirshfeld surface because the contact distance is longer than the sum of the van der Waals radii. However, the interaction energy for this stacked dimer is –9.1 kcal/mol. This is stronger than the other interactions observed in **MHE-4**. Fig. 6 indicates that the O…H intermolecular contacts (42%) in **MHE-4** are dominant than in other structures reported in this paper. The relative contributions of intermolecular O…H contacts observed in **MHE-1-3** are 27, 25 and 23%, respectively. In **MHE-4**, it is important to note that the relative contributions of intermolecular H…H contact is lower than in other four structures. The relative contribution of intermolecular C…H contacts is also slightly lower in this structure than in other four structures. The overall lattice energy for **MHE-4** structure is stronger than **MHE-1-3** structures. It is interesting to note that in the context of interacting groups, there are some commonalities between **MHE-4** and **MHE-1**–**3** structures. For example, phenyl/acid (C6–H6…O2 in **MHE-4**) and ester/acid (O3=C10…O1=C9 in **MHE-4**) interactions are retained in **MHE-1**–**4**. There are some new contacts also observed due to nitro substitution. They are found between nitro/amine and nitro/phenyl ring groups.

[Insert Figure 10]

Fig.10 Overlay diagram showing the molecule of **MHE-5** superimposed onto the one of the molecules of **MHE-1** in the dimer formed by an invariant intermolecular N–H…O hydrogen bond. The dashed lines indicate the steric clash between atom O2 of carboxylic group in **MHE-1-3** and carbonyl O5 atom of ethyl ester moiety in **MHE-5**.

Like in **MHE-4**, the intermolecular N–H…O2=C9 hydrogen bond is also altered due to ethyl ester substitution at

the *ortho* position on the phenyl ring in **MHE-5**. The structural superposition of dimeric molecules of **MHE-1** with the monomeric **MHE-5** structure gives rise to a steric hindrance. The carbonyl O5 atom of ethyl ester moiety of **MHE-5** makes steric clash with carboxylic O2 atom of **MHE-1** with a distance of 1.068 Å (Fig. 10). Apart from intramolecular N–H…O and O–H…O hydrogen bonds which generate three fused *S*(6) rings as discussed earlier, intermolecular C7–H7…O3 and C11–H11b…O2 interactions link the molecules into *C*(5) and *C*(7) chains (Fig. 11), respectively. The intermolecular interaction energy is being –4.9 kcal/mol for C7–H7…O3 and –7.0 kcal/mol for C11–H11b…O2 molecular pair. Atom C14 (via H14A) is participated in an intermolecular C–H…π interaction (Fig. 12) with the centroid atom of phenyl ring at (*1–x, –y, 1–z*). The interaction energy for this molecular pair being –7.0 kcal/mol. In the crystal structure, molecules of **MHE-5** are stacked in a zigzag fashion which runs parallel to the *a* axis.

[Insert Figure 11]

Fig. 11 Part of the crystal structure of **MHE-5,** showing the formation of *C*(5) (magenta) and *C*(7) chains (green) formed by weak intermolecular C–H…O interactions. For clarity H atoms have not been involved in interactions are removed.

[Insert Figure 12]

Fig.12. The crystal packing of **MHE-5**, showing molecular stacking interconnected by C–H…π and π …π interactions.

As shown in Fig. 12, each stacking pair is interconnected by an intermolecular C–H…π interaction and the adjacent pair is further interconnected by a π…π interaction with centroid-to-centroid distance of 4.568 Å (*2–x, –y,1–z*). The interaction energy for this π…π stacked molecular pair being –12.7 kcal/mol. The substituted ester group (C15 via H15*B*) is involved in an intermolecular C–H…O interaction with carboxylic acid moiety (atom O1). This interaction links the molecules as a dimer and the interaction energy is being –7.5 kcal/mol. This and the subsequent contacts are formed only when the sum of the van der Waals radii of the interacting atoms plus 0.1 Å criterion is considered. Atom C5 (via H5) is involved in an intermolecular C–H…O interaction with carbonyl O5 atom of substituted ester moiety. Within this pair (interaction energy is being –5.6 kcal/mol), there are two additional contacts also observed. They are H4…H14*A* and H4…C14 intermolecular contacts. The overall lattice energy for **MHE-5** is stronger than other four structures. It is interesting to note that there is an invariant contact observed between ester/acid moieties (C11–H11*B*…O2=C9) in all five structures.

Conclusions

A series of crystal structures of malonic acid half-ester derivatives with different functional groups have been determined and analysed to understand their supramolecular architectures. The crystal packing of all the structures has been analysed in a systematic way using Hirshfeld surface analysis and PIXEL energy calculation. The methyl group in **MHE-2** and chloro substitution in MHE-3 does not alter the invariable intermolecular N–H…O hydrogen bond when compared to their parent compound **MHE-1**. Interestingly the structure of MHE-2 is isomorphous with **MHE-3**, while the parent compound MHE-1 does not. The overall crystal packing is similar to that observed in **MHE-1**–**3**. However, there are some variations observed between stacking of layers in these structures. The relative contribution of intermolecular H…H contacts in **MHE-3** is substantially lower than that of **MHE-1** and **MHE-2**. This reduction is compensated by H…Cl contacts. An invariant intermolecular N–H…O hydrogen bond with $R_2^2(12)$ motif is observed in **MHE-1**–**3**. Within this loop, the intramolecular N–H…O and O–H…O hydrogen bonds generate pseudo 6-, 6-, 4-, 6-, 6-membered ring system gives rise to planarity to the molecular structure. It can be used as a new type of synthon for providing planarity to the molecule. An invariant intermolecular N–H…O hydrogen bond is altered due to the substitution of nitro group in **MHE-4** and ester moiety in **MHE-5**. Overall, there are some invariant and variable interactions between different functional groups are observed in all five structures. Furthermore, strengths of various intermolecular interaction energies for molecular pairs are quantified using PIXEL energy calculations. Interestingly, some of the unconventional contacts provide greater stability to the crystal structure when compared to classical intermolecular contacts.

Acknowledgements

The authors thank the DST–India (FIST programme) for the use of the Bruker SMART APEXII diffractometer and the 400 MHz NMR facility at the School of Chemistry, Bharathidasan University. ST is highly grateful to the management of SASTRA University for infrastructural and financial support (Prof. TRR grant). Financial support from Department of AYUSH (Z.15075/1/2010-COE), Government of India for purchase of Schrödinger suite is gratefully acknowledged.

References

1. (a) A. Nangia and G. R. Desiraju, In Design of Organic Solids, ed. E. Weber, Springer-Verlag, Berlin, 1998; (b) C. B. Aakeroy, N. R. Champness and C. Janiak, *CrystEngComm.,* 2010, **12**, 22; (c) K. Biradha, C.-Y. Su and J. Vittal, J. *Cryst. Growth Des.,* 2011, **11**, 875; (d) D. Braga, G. R. Desiraju, J. S. Miller, A. G. Orpen and S. L. Price, *CrystEngComm.,*2002, **4**, 500.

2. (a) G. R. Desiraju, *Acc. Chem. Res*., 1991, **24**, 290; (b) T. Steiner, *Crystallogr. Rev.,* 2003, **9**, 177; (c) F. C. Pigge, F. Ghasedi, Z. Zheng, N. P. Rath, G. Nichols and J. S. Chickos, *J. Chem. Soc., Perkin Trans.2.,* 2000, 2458; (d) C. M. Reddy, L. S. Reddy, S. Aitipamula, A. Nangia, C.-K. Lam and T. C. W. Mak, *CrystEngComm*., 2005, **7**, 44; (e) V. S. S. Kumar, F. C. Pigge and N. P. Rath, *Cryst.Growth Des.,* 2006, **6**, 193.

3. (a) C. V. K. Sharma, K. Panneerselvam, T. Pilati, and G. R. Desiraju, *J. Chem. Soc., Perkin Trans.2.,* 1993, 2209. (b) C. V. K. Sharma and G. R. Desiraju, *J. Chem. Soc., Perkin Trans.2.,* 1994, 2345.

4. S.K. Sureshan, and G.G. Rajesh, *CrystEngComm*., 2013, **15**, 1676

5. (a) J. V. B. Kanth and M. Periasamy, *J. Org. Chem.,* 1991, **56**, 5964.; (b) J. Baudoux, P. Lefebvre, R. Legay, M.-C. Lasne and J. Rouden, *Green Chem.,* 2010, **12**, 252.

6. S. Niwayama, *J. Org. Chem*. 2000, **65**, 5834.

7. L.J. Durham, D. J. McLeod and J. Cason, *Org. Synth*. 1963, **4**, 635.

8. S. J. Pridmore and J. M. J. Williams, *Tetrahedron Lett.,* 2008, **49**,7413.

9. Y. Ryu and A. I. Scott, *Tetrahedron Lett.,* 2003, **44**, 7499.

10. L.R. Wiseman and D. McTavish, *Drugs*. 1994, **48**, 71.

11. A. Nahum, A. Erhart, D. Gazard, C. Agbowai, C.V. Overmeir, H. van Loen, J. Menten, M. Akogbeto, M. Coosemans, A. Massougbodji and U. D'Alessandro. *Malaria Journal*. 2007, **6**, 170.

12. (a) J. J. McKinnon, D. Jayatilaka and M.A. Spackman, *Chem. Commun.,* 2007, 3814; (b) M.A. Spackman, D. Jayatilaka, *CrystEngComm.,* 2009, **11**, 19.

13. (a) M.A. Spackman, J.J. McKinnon, *CrystEngComm.,* 2002, **4**, 378; (b) J.J. McKinnon, M.A. Spackman, A.S. Mitchell, *Acta Cryst.,* 2004, **B60**, 627; (c) J. J. McKinnon, D. Jayatilaka and M. A. Spackman, *Chem. Commun.,* 2007, 3814.

14. (a) A. Gavezzotti, *New J. Chem.,* 2011, **35**, 1360; (b) A. Gavezzotti, *J. Phys. Chem. B,*2003, **107**, 2344; (c) A. Gavezzotti, *J. Phys. Chem. B,* 2002, **106**, 4145.

15. (a) A. D. Becke, *J. Chem. Phys.,* 1993, **98**, 5648; (b) C. T. Lee, W. T. Yang and R. G. Parr, *Phys. Rev. B: Condens. MatterMater. Phys.,* 1998, **37**, 1133.

16. A. Ilangovan, R.Ganesh kumar, and M. P. Kaushikb, *Synlett*., 2012, **23**, 2093.

17. Bruker, *APEX2*, *SAINT* and *SADABS*, Bruker AXS Inc., Madison, 50 Wisconsin, USA, 2008.

18. G. M. Sheldrick, *Acta Cryst.* 2008, **A64**, 112.

19. L. J. Farrugia, *J. Appl. Cryst.* 2012, **45**, 849.

20. A. L. Spek, *Acta Cryst.* 2009, **D65**, 148.

21. C.F. Macrae, P. R. Edgington, P. McCabe, E. Pidcock, G. P.Shields, R. Taylor, M. Towler and J. van de Streek, *J. Appl. Cryst.* 2006, **39**, 453.

22. T. Gelbrich, T. L. Threlfall, S. Huth, E. Seeger and M. B. Hursthouse, *Z. Anorg. Allg. Chem.*, 2004, **630**, 1451.

23. Schrödinger Release 2013–3: Jaguar, version 8.2, Schrödinger, LLC, New York, NY, (2013).

24. Schrödinger Release 2013–3: Maestro, version 9.6, Schrödinger, LLC, New York, NY, (2013).

25. S. K. Wolff, D. J. Grimwood, J. J. McKinnon, M. J. Turner, D. Jayatilaka and M. A. Spackman, Crystal Explorer (Version 3.0), University of Western Australia, 2012.

26. M. J. Frisch, G. W. Trucks, H. B. Schlegel, G. E. Scuseria, M. A. Robb, J. R. Cheeseman, G. Scalmani, V. Barone, B. Mennucci, G. A. Petersson, H. Nakatsuji, M. Caricato, X. Li, H. P. Hratchian, A. F. Izmaylov, J. Bloino, G. Zheng, J. L. Sonnenberg, M. Hada, M. Ehara, K. Toyota, R. Fukuda, J. Hasegawa, M. Ishida, T. Nakajima, Y. Honda, O. Kitao, H. Nakai, T. Vreven, J. A. Montgomery, Jr., J. E. Peralta, F. Ogliaro, M. Bearpark, J. J. Heyd, E. Brothers, K. N. Kudin, V. N. Staroverov, T. Keith, R. Kobayashi, J. Normand, K. Raghavachari, A. Rendell, J. C. Burant, S. S. Iyengar, J. Tomasi, M. Cossi, N. Rega, J. M. Millam, M. Klene, J. E. Knox, J. B. Cross, V. Bakken, C. Adamo, J. Jaramillo, R. Gomperts, R. E. Stratmann, O. Yazyev, A. J. Austin, R. Cammi, C. Pomelli, J. W. Ochterski, R. L. Martin, K. Morokuma, V. G. Zakrzewski, G. A. Voth, P. Salvador, J. J. Dannenberg, S. Dapprich, A. D. Daniels, O. Farkas, J. B. Foresman, J. V. Ortiz, J. Cioslowski, and D. J. Fox. Gaussian 09, revision D.01; Gaussian, Inc., Wallingford, CT, (2013).

27. J. Bernstein, R. E. Davis, L. Shimoni and N. -L. Chang, *Angew. Chem. Int. Ed. Engl.,* 1995, **34**, 1555.

28. (search filters: R-factor: ≤ 0.5%, not disordered and only organic)

29. CSD search version 5.35 2013 updates

30. K. Helttunen, L. Lehtovaara, H. Häkkinen and M. Nissinen, *Cryst. Growth Des.,* 2013, **13**, 3603 and reference cited there in.

31. V. Bertolasi, P. Gilli, V. Ferretti, G. Gilli, K. Vaughan and J. V. Jollimore, *Acta Crystallogr. Sect. B: Struct. Sci.,*1999, **B55**, 994.

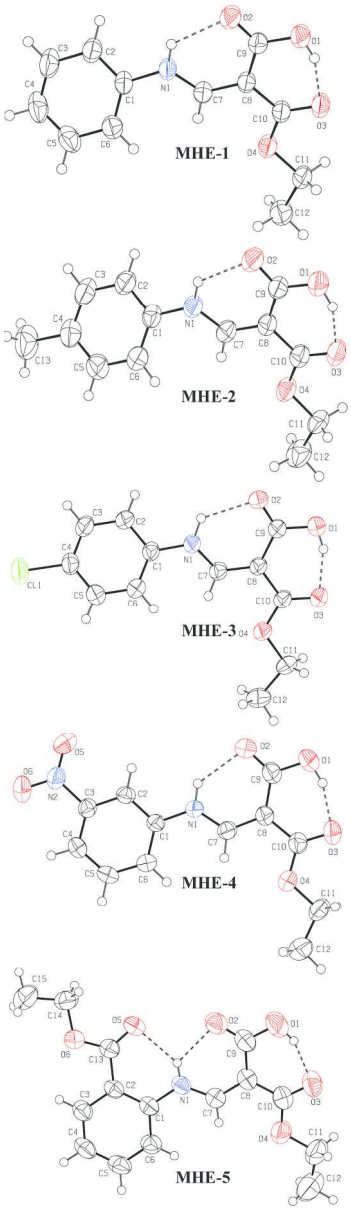

246x861mm (300 x 300 DPI)

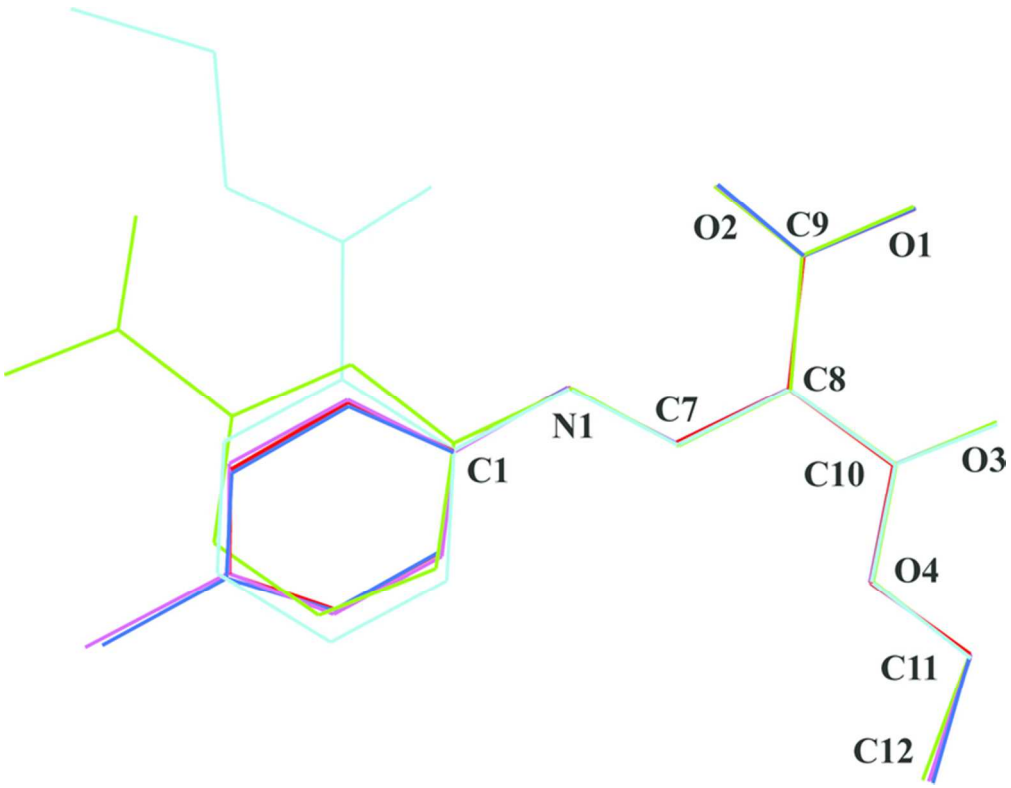

69x54mm (300 x 300 DPI)

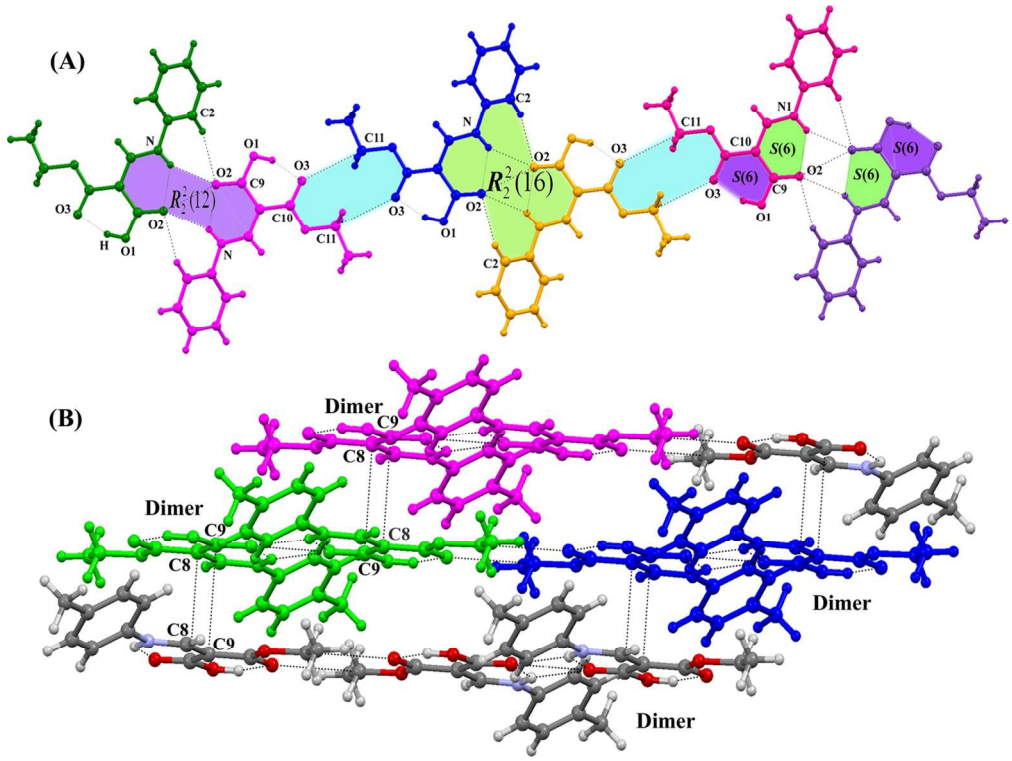

130x97mm (300 x 300 DPI)

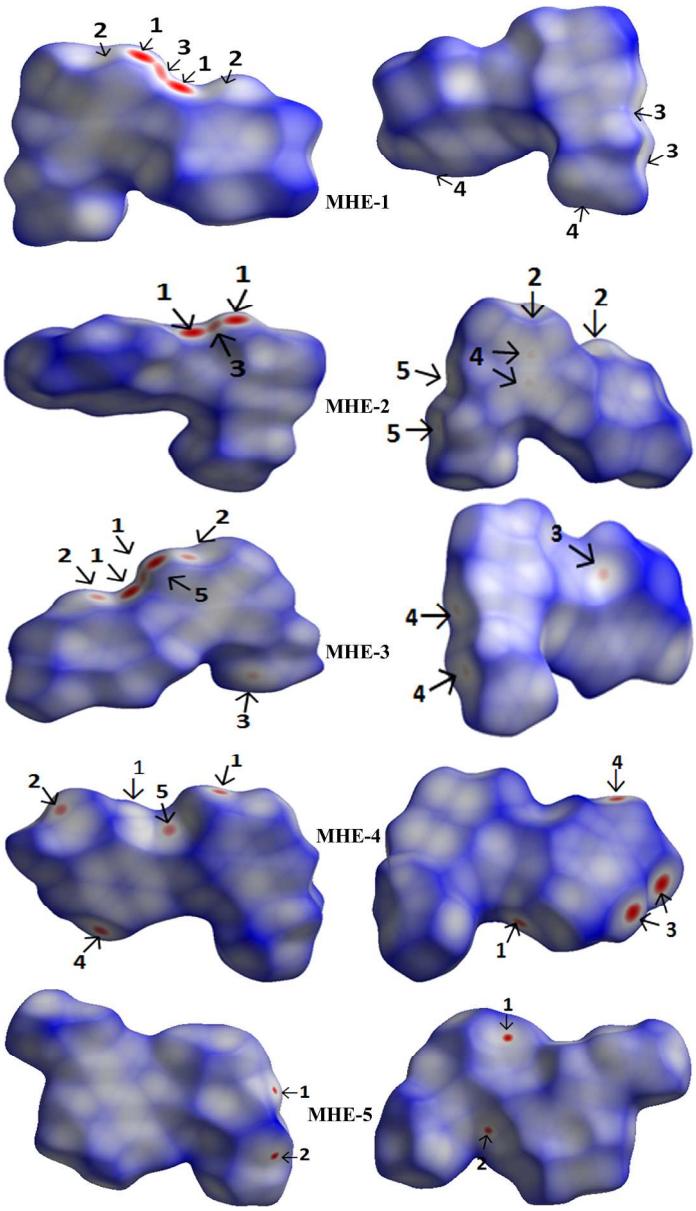

228x396mm (300 x 300 DPI)

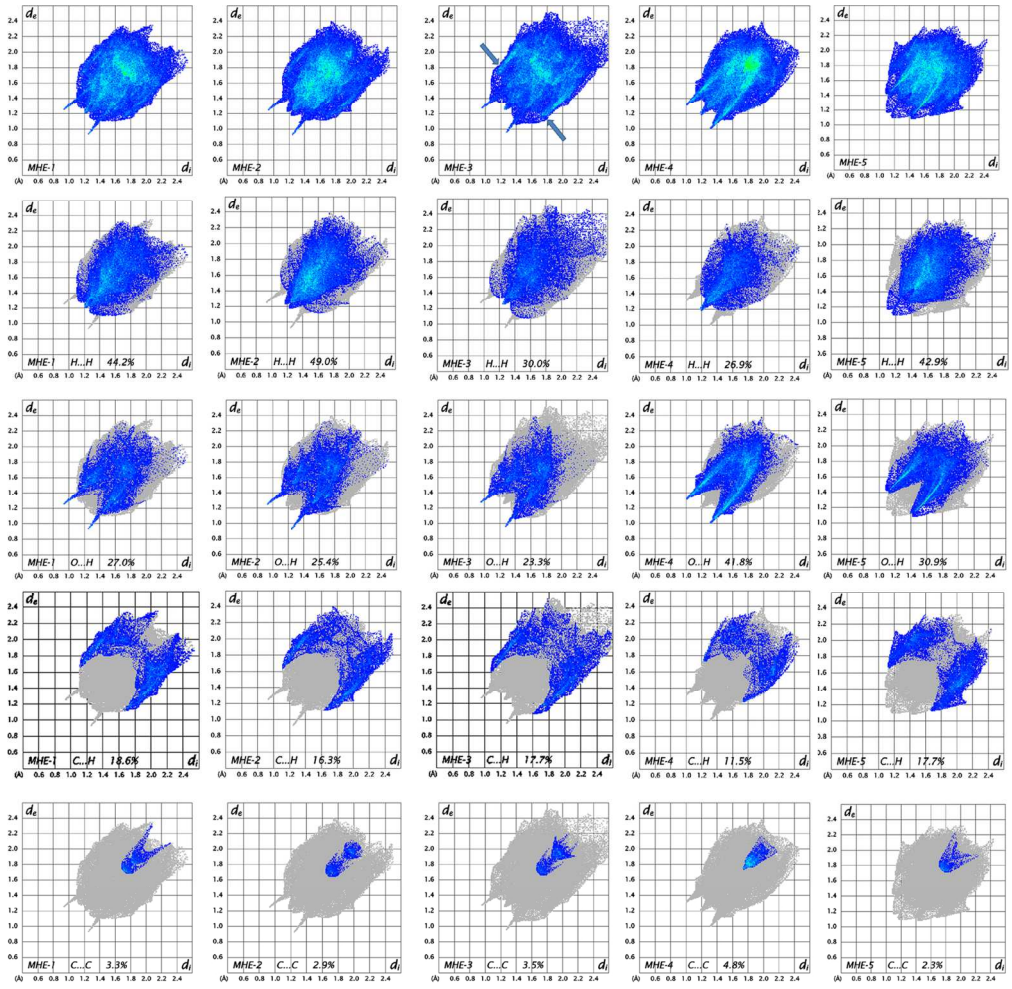

155x151mm (300 x 300 DPI)

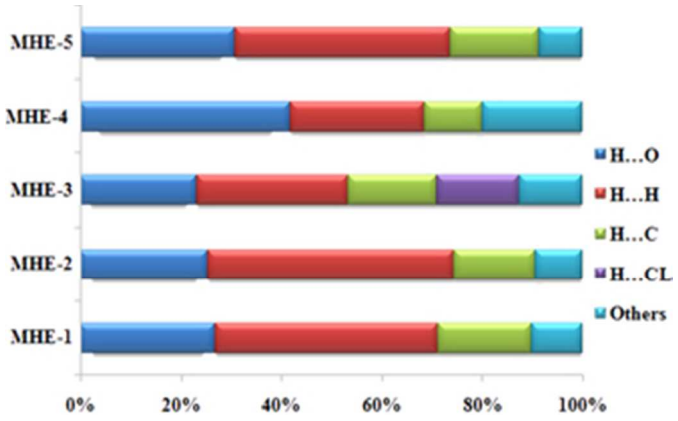

28x17mm (300 x 300 DPI)

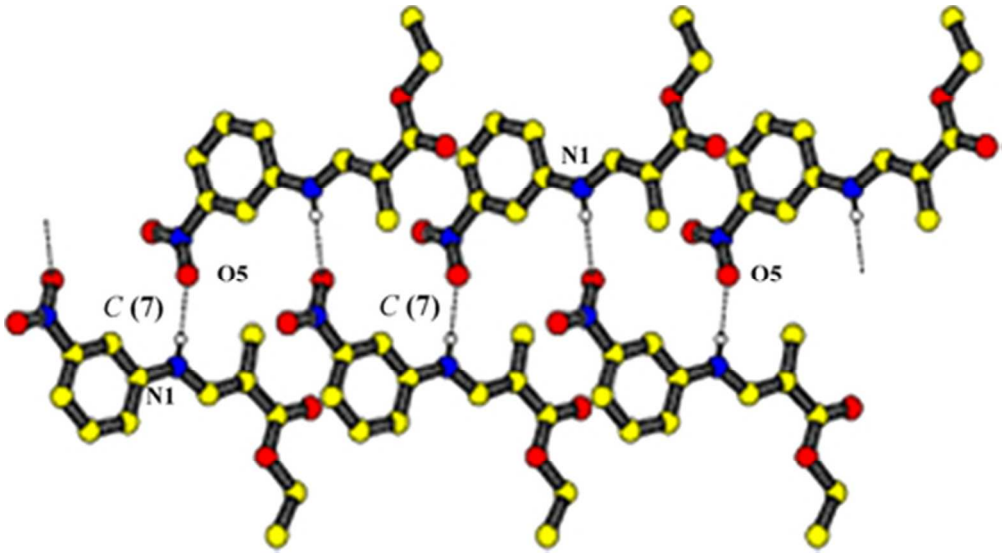

42x23mm (300 x 300 DPI)

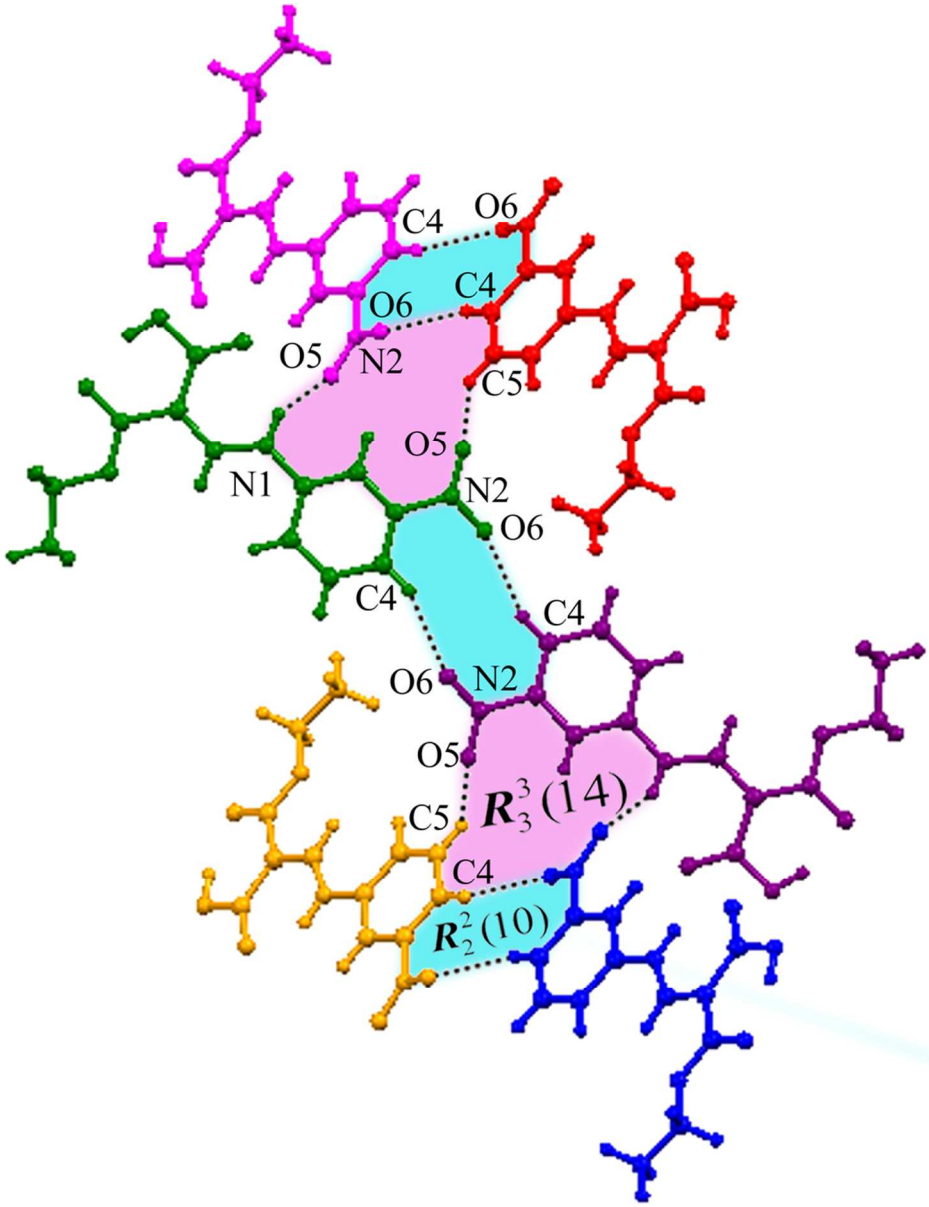

92x116mm (300 x 300 DPI)

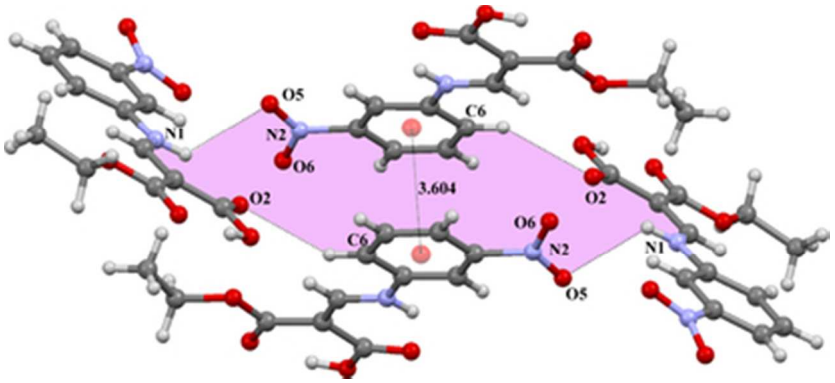

34x15mm (300 x 300 DPI)

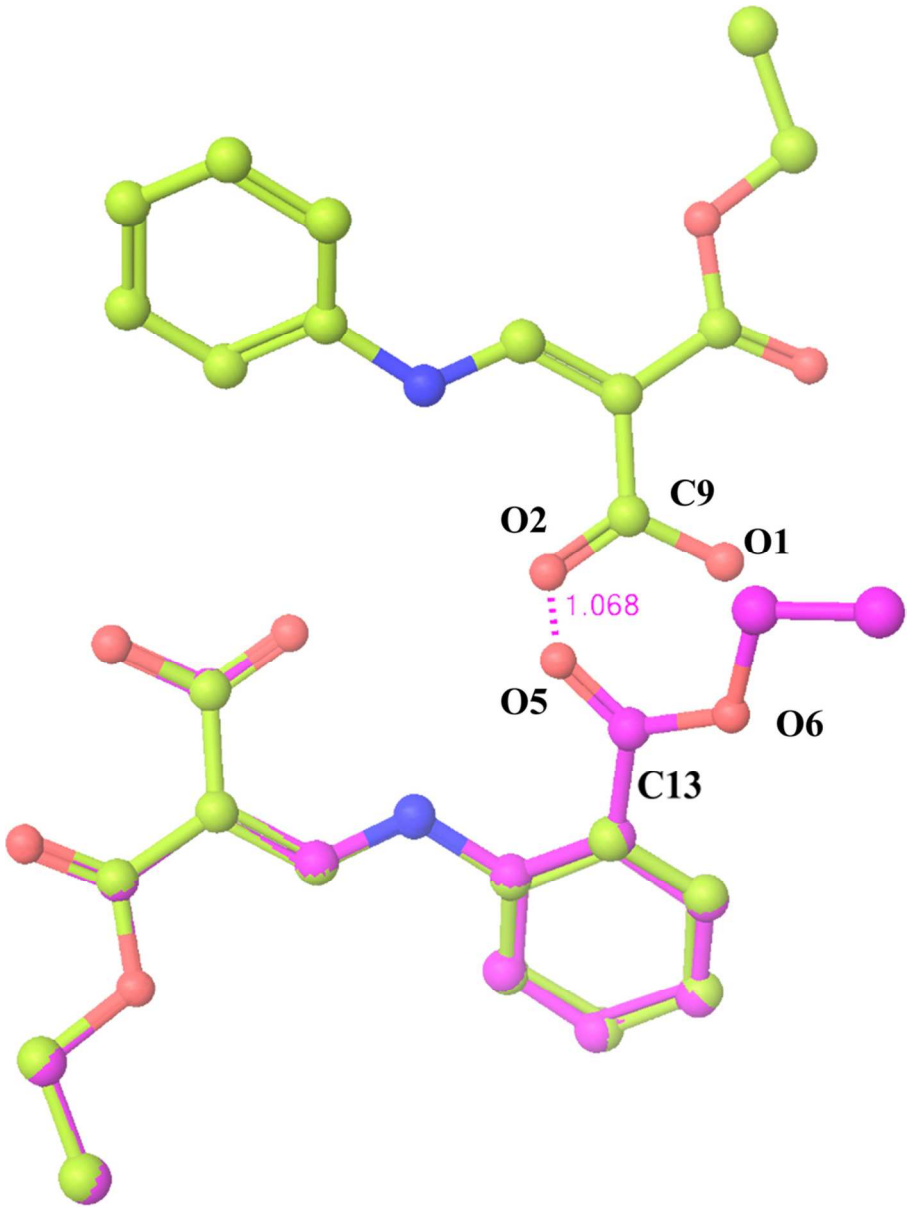

83x110mm (300 x 300 DPI)

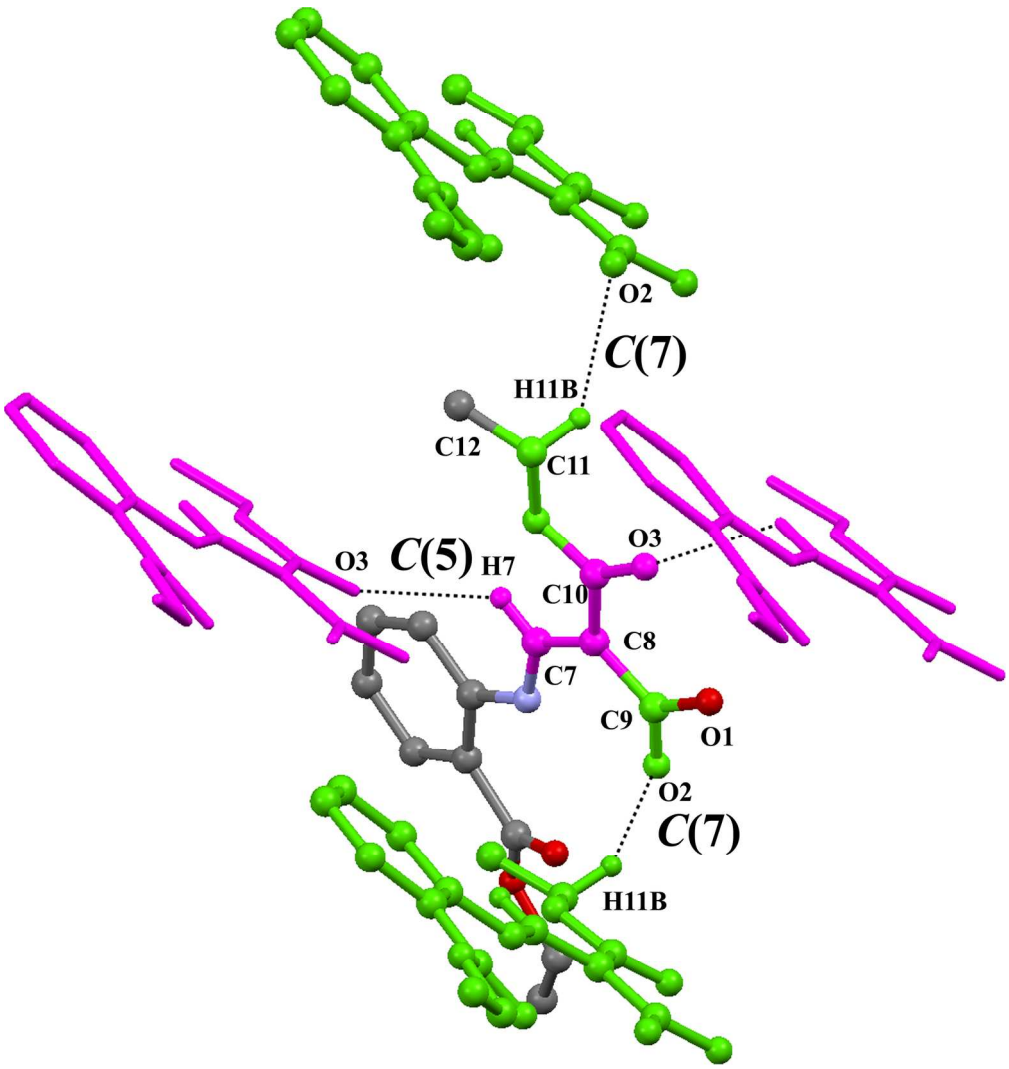

167x176mm (300 x 300 DPI)

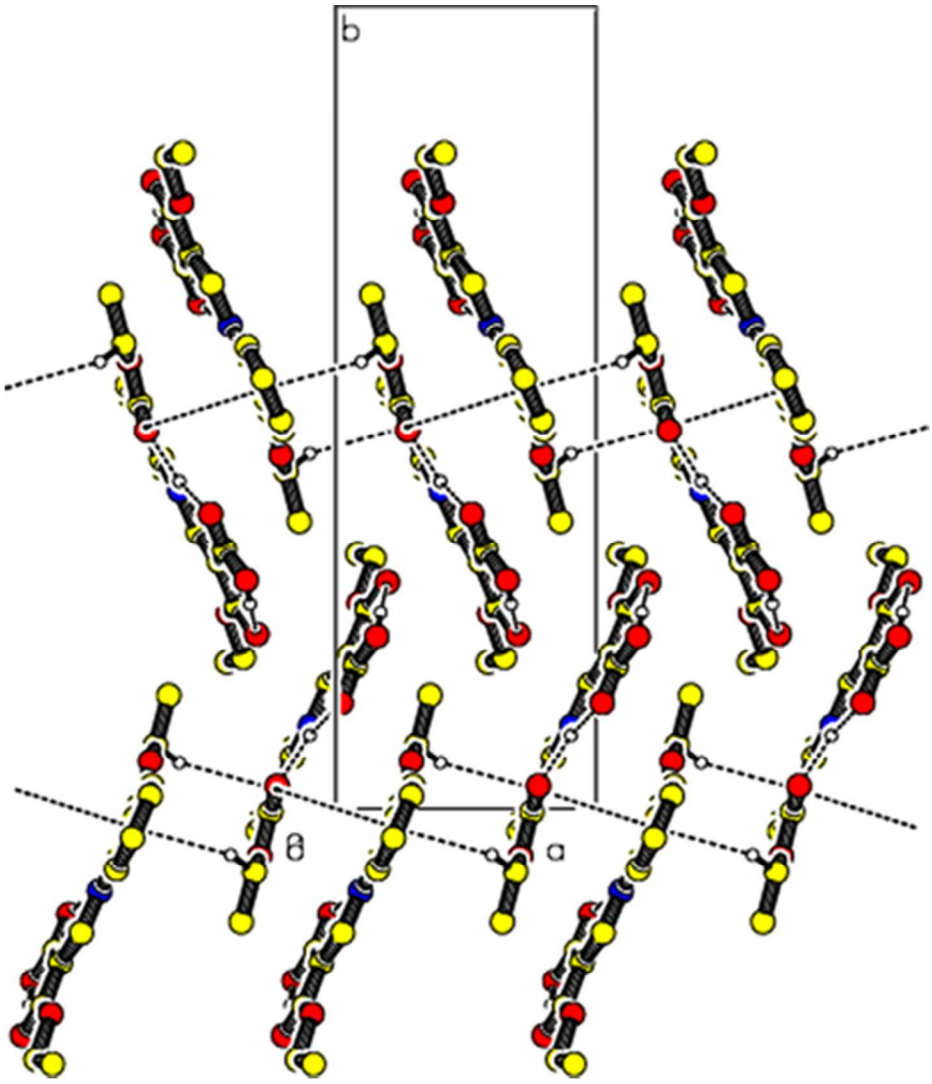

39x45mm (300 x 300 DPI)

Invariant and variable intermolecular interactions in functionalized malonic acid half-esters: X-ray, Hirshfeld surfaces and PIXEL energy analyses†

Perumal Venkatesan,[a] Subbiah Thamotharan,[b] Rajendran Ganesh Kumar[a] and Andivelu Ilangovan[a*]

A series of functionalized malonic acid half-ester derivatives have been synthesized and their crystal structures are determined. Invariant and variable intermolecular interactions in these derivatives are analysed using Hirshfeld surfaces and PIXEL energy calculations.

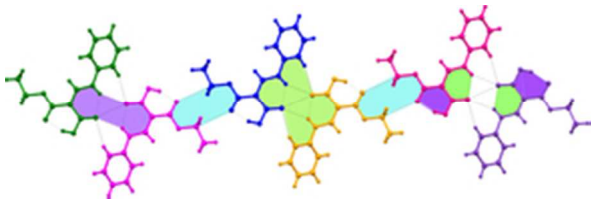

24x8mm (300 x 300 DPI)